

MAGNETIC PRANDTL NUMBER DEPENDENCE OF THE KINETIC-TO-MAGNETIC DISSIPATION RATIO

AXEL BRANDENBURG

Nordita, KTH Royal Institute of Technology and Stockholm University, SE-10691 Stockholm, Sweden

Department of Astronomy, Stockholm University, SE-10691 Stockholm, Sweden

Received 2014 April 28; accepted 2014 June 17; published 2014 July 21

ABSTRACT

Using direct numerical simulations of three-dimensional hydromagnetic turbulence, either with helical or non-helical forcing, we show that the kinetic-to-magnetic energy dissipation ratio always increases with the magnetic Prandtl number, i.e., the ratio of kinematic viscosity to magnetic diffusivity. This dependence can always be approximated by a power law, but the exponent is not the same in all cases. For non-helical turbulence, the exponent is around $1/3$, while for helical turbulence it is between 0.6 and $2/3$. In the statistically steady state, the rate of energy conversion from kinetic into magnetic by the dynamo must be equal to the Joule dissipation rate. We emphasize that for both small-scale and large-scale dynamos, the efficiency of the energy conversion depends sensitively on the magnetic Prandtl number, and thus on the microphysical dissipation process. To understand this behavior, we also study shell models of turbulence and one-dimensional passive and active scalar models. We conclude that the magnetic Prandtl number dependence is qualitatively best reproduced in the one-dimensional model as a result of dissipation via localized Alfvén kinks.

Key words: accretion, accretion disks – hydrodynamics – magnetohydrodynamics (MHD) – shock waves – turbulence

Online-only material: color figures

1. INTRODUCTION

One of the central paradigms of hydrodynamic turbulence is the equivalence of large-scale energy injection and small-scale dissipation into heat through viscosity—regardless of how small its value. This is believed also to apply under conditions of astrophysically large Reynolds numbers, when the microphysical viscosity becomes very small compared with the product of the physical scales and velocities of the system. Dramatic examples are quasars, whose luminosities are equal to that of a hundred galaxies and this emission is caused just by the dissipation of turbulence, even though the microphysical viscosity is extremely small. The detailed physical processes are not well understood, but it is now generally believed that they also involve magnetic fields (Shakura & Sunyaev 1973; Balbus & Hawley 1998).

Indeed, magnetic fields provide an additional important pathway for dissipating turbulent energy through Joule heating. The heating rates for both viscous and Joule dissipation are proportional to the microphysical values of viscosity ν and magnetic diffusivity η , respectively. The ratio of these coefficients is the magnetic Prandtl number, $\text{Pr}_M = \nu/\eta$. As these coefficients are decreasing, the velocity and magnetic field gradients sharpen just enough so that the heating rates remain independent of these coefficients. For the magnetic case of Joule heating, the independence of the magnetic Reynolds number was demonstrated by Galsgaard & Nordlund (1996) and Hendrix et al. (1996) in connection with the coronal heating problem. Over a range of magnetic Reynolds numbers, the approximate constancy of Joule dissipation has also been seen in turbulent dynamo simulations (Candelaresi et al. 2011).

While this picture is appealing and seemingly well confirmed, at least in special cases such as for fixed values of Pr_M , questions have arisen in those cases when the magnetic and fluid Reynolds numbers are changed in such a way that their ratio changes. Hydromagnetic turbulence simulations exhibiting dynamo action have shown that the values of energy dissipation

are then no longer constant, and that their ratio scales with Pr_M (Mininni 2007; Brandenburg 2009, 2011a, 2011b). Given that all of the energy that is eventually dissipated comes from the forcing in the momentum equation, a change in the dissipation ratio can only be a consequence of a change in the conversion of kinetic to magnetic energy through the dynamo process. Therefore, the dynamo process would be intimately linked to Joule dissipation and one must therefore be concerned that it is also linked to the physical or even numerical nature of energy dissipation. This would be surprising, because dynamo action has frequently been modeled in many astrophysical turbulence simulations by focusing on the so-called ideal equations with numerical dissipation only where no Pr_M can be defined. Examples in the context of local accretion disk dynamo simulations can be found in the papers by Brandenburg et al. (1995), Hawley et al. (1996), and Stone et al. (1996). This leads to an ignorance that is potentially dangerous if such simulations are employed to make predictions concerning energy deposition in accretion disks (see discussion by Bisnovatyi-Kogan & Lovelace 1997).

There is some concern that the numerical results of Brandenburg (2009, 2011a) may not yet be in the asymptotic regime and that the Pr_M dependence might disappear at sufficiently large values of Re . However, two arguments against this possibility have now emerged. First, there are analytic results in two-dimensional magnetohydrodynamics (MHD) by Tran et al. (2013) that demonstrate the boundedness of the mean-squared current density and mean-squared vorticity in the limits of large and small values of Pr_M , respectively. In fact, Tran et al. (2013) also produce numerical scalings similar to the results of Brandenburg (2011a, 2011b). Second, MHD shell models of turbulence by Plunian & Stepanov (2010) for $\text{Pr}_M > 1$ show a similar Pr_M dependence, which is remarkable because those models can be extended to much larger values of Re_M than what is currently possible with DNS.

Thus, there is now mounting evidence for a genuine dependence of the macroscopic properties of MHD turbulence on Pr_M . Another such dependence has been discussed for some time in

connection with non-helical turbulence exhibiting small-scale dynamo action in the *kinematic* regime. Note, however, that this no longer applies in the non-kinematic regime (Brandenburg 2011a). For a kinematic small-scale dynamo, the magnetic energy spectra grow in an approximately shape-invariant fashion with an approximate $k^{3/2}$ spectrum at small wavenumbers. This spectrum was first predicted by Kazantsev (1968) in the case of a smooth flow. This case corresponds to an idealized representation of turbulence at large values of Pr_M (Schekochihin et al. 2002), but this spectrum is apparently also found at small values of Pr_M near unity (see Figure 4 of Haugen et al. 2004). Depending on the value of Pr_M , the magnetic energy spectrum peaks at wavenumbers either within the inertial range of the turbulence or in the viscous subrange. This has implications for the critical magnetic Reynolds number for the onset of dynamo action (Rogachevskii & Kleeorin 1997). As explained by Boldyrev & Cattaneo (2004), the velocity field is rough in the inertial range. This interpretation has been successfully applied when clarifying the reason for an apparent divergence (Schekochihin et al. 2005) of the critical Reynolds number above which dynamo action is possible (Iskakov et al. 2007; Schekochihin et al. 2007).

There has been a similar debate regarding the onset of magneto-rotational instability in local simulations of accretion disks (Fromang & Papaloizou 2007; Fromang et al. 2007), where the instability was found not to be excited for small values of Pr_M . However, these examples are restricted to the physics of small-scale magnetic fields only. If one allows large-scale fields to develop, e.g., by relaxing the restriction to closed or periodic boundary conditions, this Pr_M dependence disappears (Käpylä & Korpi 2011).

In the following, we will be concerned with the fully dynamic case where kinetic and magnetic energies are comparable. The purpose of the present paper is to illuminate the problem of the Pr_M dependence of the dissipation ratio through a combination of different approaches to MHD turbulence ranging from direct numerical simulations (DNS) of the MHD equations in three dimensions and shell models of the turbulence capturing aspects of the spectral cascade, to a simple one-dimensional model of MHD (see Thomas 1968; Pouquet 1993; Basu et al. 2014). This leads us to suggest that the Pr_M dependence found in turbulent dynamo simulations is caused by the dominant influence of dissipative structures on the turbulent cascade at larger scales. These dissipative structures can be thought of as local Alfvén kinks whose width is determined by the algebraic mean of kinematic viscosity and magnetic diffusivity.

2. SIMULATIONS OF TURBULENT DYNAMOS

2.1. Governing Equations

In this section, we consider forced MHD turbulence of a gas that can be described by an isothermal equation of state, i.e., the gas pressure p is proportional to the gas density ρ with $p = \rho c_s^2$, where $c_s = \text{const}$ is the isothermal sound speed. We apply a forcing function \mathbf{f} that is either fully helical or non-helical. In both cases, there is initially just a weak seed magnetic field, which is then amplified by dynamo action. In the former case with helicity, we obtain large-scale magnetic fields, as were studied previously with similar setups (Brandenburg 2001, 2009; Mininni 2007), while in the latter case only small-scale dynamo action is possible (Cho & Vishniac 2000; Haugen et al. 2003, 2004; Schekochihin et al. 2004; Brandenburg 2011a). In some cases, we also include the Coriolis force to study the

effects of rotation. We solve the governing equations in the form

$$\frac{D \ln \rho}{Dt} = -\nabla \cdot \mathbf{u}, \quad (1)$$

$$\frac{D\mathbf{u}}{Dt} = -c_s^2 \nabla \ln \rho - 2\boldsymbol{\Omega} \times \mathbf{u} + \mathbf{f} + \rho^{-1} [\mathbf{J} \times \mathbf{B} + \nabla \cdot (2\nu\rho\mathbf{S})], \quad (2)$$

$$\frac{\partial \mathbf{A}}{\partial t} = \mathbf{u} \times \mathbf{B} - \eta\mu_0 \mathbf{J}, \quad (3)$$

where $D/Dt = \partial/\partial t + \mathbf{u} \cdot \nabla$ is the advective derivative, \mathbf{u} is the velocity, $\mathbf{B} = \nabla \times \mathbf{A}$ is the magnetic field, \mathbf{A} is the magnetic vector potential, $\mathbf{J} = \nabla \times \mathbf{B}/\mu_0$ is the current density, μ_0 is the vacuum permeability, and

$$\mathbf{S}_{ij} = \frac{1}{2}(u_{i,j} + u_{j,i}) - \frac{1}{3}\delta_{ij}\nabla \cdot \mathbf{u} \quad (4)$$

is the traceless rate-of-strain tensor. It is useful to note that

$$\rho^{-1}\nabla \cdot (2\rho\mathbf{S}) = \frac{4}{3}\nabla\nabla \cdot \mathbf{u} - \nabla \times \nabla \times \mathbf{u} + 2\mathbf{S} \cdot \nabla \ln \rho, \quad (5)$$

where we call attention to the presence of the 4/3 factor which will be relevant for irrotational flows.

We consider a triply periodic domain, so that the kinetic and magnetic energy balance is described by

$$\frac{d}{dt}\langle \rho\mathbf{u}^2/2 \rangle = \langle p\nabla \cdot \mathbf{u} \rangle + \langle \mathbf{u} \cdot (\mathbf{J} \times \mathbf{B}) \rangle + \langle \rho\mathbf{u} \cdot \mathbf{f} \rangle - \langle 2\rho\nu\mathbf{S}^2 \rangle, \quad (6)$$

$$\frac{d}{dt}\langle \mathbf{B}^2/2\mu_0 \rangle = -\langle \mathbf{u} \cdot (\mathbf{J} \times \mathbf{B}) \rangle - \langle \eta\mu_0\mathbf{J}^2 \rangle, \quad (7)$$

where $\mathbf{S}^2 = \mathbf{S}_{ij}\mathbf{S}_{ji}$. The total (kinetic plus magnetic) energy is sourced by $\langle \rho\mathbf{u} \cdot \mathbf{f} \rangle$ and dissipated by the sum of viscous and Joule dissipation, $\epsilon_T = \epsilon_K + \epsilon_M$, with

$$\epsilon_K = \langle 2\rho\nu\mathbf{S}^2 \rangle \quad \text{and} \quad \epsilon_M = \langle \eta\mu_0\mathbf{J}^2 \rangle. \quad (8)$$

The terms $\langle p\nabla \cdot \mathbf{u} \rangle$ and $\langle \mathbf{u} \cdot (\mathbf{J} \times \mathbf{B}) \rangle$ characterize the work done by gas expansion and Lorentz force, respectively.

A sketch showing the transfers in and out of the two energy reservoirs, $E_K = \langle \rho\mathbf{u}^2/2 \rangle$ and $E_M = \langle \mathbf{B}^2/2\mu_0 \rangle$, is given in Figure 1. From this it is clear that in the steady state, the quantity $-\langle \mathbf{u} \cdot (\mathbf{J} \times \mathbf{B}) \rangle$ must be positive and equal to $\langle \eta\mu_0\mathbf{J}^2 \rangle$.

2.2. The Model

We solve Equations (1)–(3) with periodic boundary conditions using the PENCIL CODE,¹ which employs sixth-order finite differences and a third-order accurate time stepping scheme. For most of our runs, we choose a resolution of 512^3 meshpoints.

In all cases, the amplitude of the forcing function is $f_0 = 0.02$, which results in a Mach number u_{rms}/c_s of around 0.1. Here, u_{rms} is the rms value of the resulting velocity. The simulations are further characterized by the fluid and magnetic Reynolds numbers,

$$\text{Re} = u_{\text{rms}}/\nu k_f, \quad \text{Re}_M = u_{\text{rms}}/\eta k_f, \quad (9)$$

so $\text{Pr}_M = \text{Re}_M/\text{Re}$. In cases with rotation, we also specify the Coriolis number:

$$\text{Co} = 2\boldsymbol{\Omega}/u_{\text{rms}}k_f. \quad (10)$$

¹ <http://pencil-code.googlecode.com/>

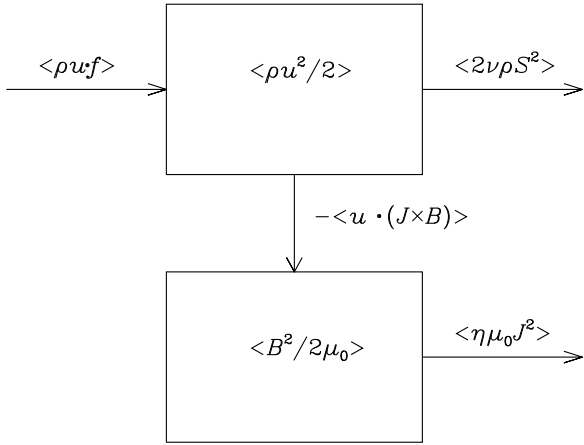


Figure 1. Sketch showing the flow of energy injected by the forcing $\langle \rho \mathbf{u} \cdot \mathbf{f} \rangle$ and eventually dissipated viscously and resistively via the terms ϵ_K and ϵ_M . Note that in the steady state, ϵ_M must be balanced by $-\langle \mathbf{u} \cdot (\mathbf{J} \times \mathbf{B}) \rangle$.

The energy supply for a helically driven dynamo is provided by the forcing function $\mathbf{f} = \mathbf{f}(\mathbf{x}, t)$, which is random in time and defined as

$$\mathbf{f}(\mathbf{x}, t) = \text{Re}\{N \mathbf{f}_{\mathbf{k}(t)} \exp[i\mathbf{k}(t) \cdot \mathbf{x} + i\phi(t)]\}, \quad (11)$$

where \mathbf{x} is the position vector. The wavevector $\mathbf{k}(t)$ and the random phase $-\pi < \phi(t) \leq \pi$ change at every time step, so $\mathbf{f}(\mathbf{x}, t)$ is δ -correlated in time. Therefore, the normalization factor N has to be proportional to $\delta t^{-1/2}$, where δt is the length of the time step. On dimensional grounds, we choose $N = f_0 c_s (|\mathbf{k}| c_s / \delta t)^{1/2}$, where f_0 is a non-dimensional forcing amplitude. We use $f_0 = 0.02$, which results in a maximum Mach number of about 0.3 and an rms value of about 0.085. At each timestep, we randomly select one of many possible wavevectors in a certain range around a given forcing wavenumber with an average value k_f . Transverse helical waves are produced via (Brandenburg & Subramanian 2005)

$$\mathbf{f}_{\mathbf{k}} = \mathbf{R} \cdot \mathbf{f}_{\mathbf{k}}^{(\text{nohel})} \quad \text{with} \quad R_{ij} = \frac{\delta_{ij} - i\sigma \epsilon_{ijk} \hat{k}_k}{\sqrt{1 + \sigma^2}}, \quad (12)$$

where σ is a measure of the helicity of the forcing and $\sigma = 1$ for positive maximum helicity of the forcing function, and

$$\mathbf{f}_{\mathbf{k}}^{(\text{nohel})} = (\mathbf{k} \times \hat{\mathbf{e}}) / \sqrt{\mathbf{k}^2 - (\mathbf{k} \cdot \hat{\mathbf{e}})^2} \quad (13)$$

is a non-helical forcing function, where $\hat{\mathbf{e}}$ is an arbitrary unit vector that is not aligned with \mathbf{k} ; note that $|\mathbf{f}_{\mathbf{k}}|^2 = 1$ and

$$\mathbf{f}_{\mathbf{k}} \cdot (i\mathbf{k} \times \mathbf{f}_{\mathbf{k}})^* = 2\sigma k / (1 + \sigma^2), \quad (14)$$

so the relative helicity of the forcing function in real space is $2\sigma / (1 + \sigma^2)$; see Candelaresi & Brandenburg (2013). In the cases mentioned below, we choose $k_f/k_1 = 3.1$ when $\sigma = 1$, so as to allow sufficient scale separation for the large-scale field to develop, and $k_f/k_1 = 1.5$ when $\sigma = 0$, where the issue of scale separation is presumably less critical.

2.3. Results

In Table 1, we present a summary of the runs discussed in this paper. As in Brandenburg (2011a), ϵ_K and ϵ_M are normalized by their sum, $\epsilon_T = \epsilon_K + \epsilon_M$, which in turn is expressed in terms

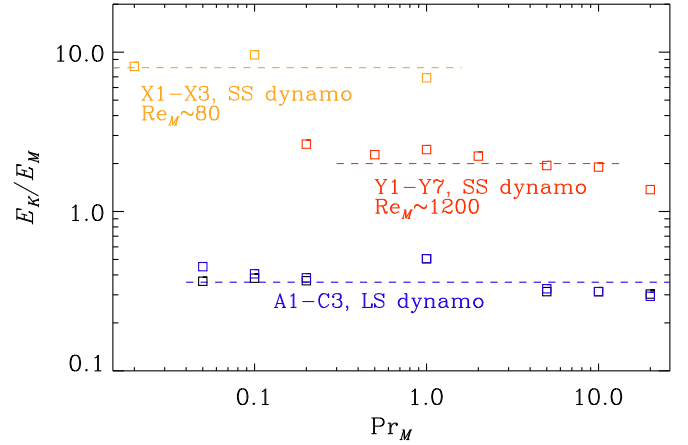


Figure 2. Dependence of the ratio E_K/E_M on Pr_M for large-scale (LS) dynamos (solid blue line, Runs A1–C3) and small-scale (SS) dynamos (dashed orange and red lines, Runs X1–Y7).

(A color version of this figure is available in the online journal.)

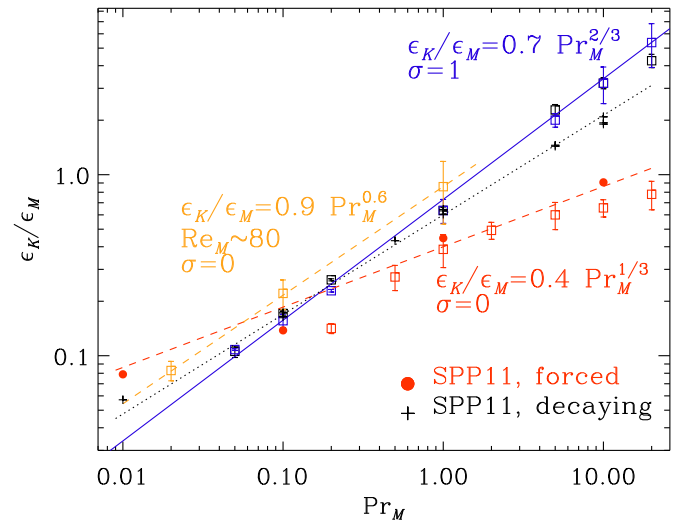


Figure 3. Dependence of the dissipation ratio ϵ_K/ϵ_M on Pr_M for large-scale dynamos (solid blue line) and small-scale dynamos (dashed orange and red lines). The red filled symbols and black plus signs correspond to the results of Sahoo et al. (2011) for forced and decaying turbulence, respectively, referred to as SPP11 in the legend.

(A color version of this figure is available in the online journal.)

of the non-dimensional quantity $C_\epsilon = \alpha \epsilon_T / \langle \rho u_{\text{rms}}^3 k_f \rangle$, where $\alpha = 9\pi\sqrt{3}/4 \approx 12.2$ is a coefficient. First of all, note that in all cases, the energy ratio E_K/E_M is roughly independent of Pr_M but it varies with Re_M , as was demonstrated previously for the small-scale dynamo (Haugen et al. 2003). For large-scale dynamos, the ratio E_K/E_M is essentially equal to k_1/k_f (Brandenburg 2001), which is around 0.3 in the present case (see Figure 2). In Figure 3, we show the Pr_M dependence of ϵ_K/ϵ_M for $\sigma = 1$ and 0. The simulations show that for both $\sigma = 1$ and 0, the ratio ϵ_K/ϵ_M scales with Pr_M ,

$$\epsilon_K/\epsilon_M \propto \text{Pr}_M^q, \quad (15)$$

but the exponent is not always the same. For $\sigma = 1$, we find $q \approx 2/3$ for both small and large values of Pr_M , while for $\sigma = 0$, we find $q \approx 0.6$ for $\text{Pr}_M < 1$ with $\text{Re} \approx 80$ and $q \approx 0.3$ for $\text{Pr}_M > 1$ with $\text{Re} \approx 460$. For large-scale dynamos ($\sigma = 1$), a similar scaling was first found for $\text{Pr}_M \leq 1$ (Mininni 2007; Brandenburg 2009), and later also for $\text{Pr}_M \geq 1$ (Brandenburg

Table 1
Summary of Runs with $Co = 0$

Run	$\nu k_1/c_s$	$\eta k_1/c_s$	Re	Re_M	Pr_M	σ	u_{rms}/c_s	b_{rms}/c_s	ϵ_K/ϵ_T	ϵ_M/ϵ_T	C_ϵ	k_v/k_1	k_η/k_1	res.
A1	5.0×10^{-4}	2.5×10^{-5}	56	1123	20.00	1	0.087	0.158	0.81	0.19	1.83	38	247	1024 ³
A2	5.0×10^{-4}	5.0×10^{-5}	57	568	10.00	1	0.088	0.157	0.76	0.24	1.80	37	156	512 ³
A3	5.0×10^{-4}	1.0×10^{-4}	57	284	5.00	1	0.088	0.157	0.69	0.31	1.82	36	99	512 ³
A4	5.0×10^{-5}	5.0×10^{-5}	587	587	1.00	1	0.091	0.128	0.39	0.61	1.75	179	201	512 ³
A5	5.0×10^{-5}	2.5×10^{-4}	606	121	0.20	1	0.094	0.155	0.21	0.79	1.46	150	63	512 ³
A6	5.0×10^{-5}	5.0×10^{-4}	594	59	0.10	1	0.092	0.149	0.15	0.85	1.60	139	38	512 ³
A7	5.0×10^{-5}	1.0×10^{-3}	581	29	0.05	1	0.090	0.149	0.10	0.90	1.72	125	23	512 ³
B1	5.0×10^{-5}	5.0×10^{-5}	587	587	1.00	1	0.091	0.128	0.39	0.61	1.75	179	201	512 ³
B2	2.5×10^{-4}	5.0×10^{-5}	117	587	5.00	1	0.091	0.159	0.67	0.33	1.57	60	168	512 ³
B3	5.0×10^{-4}	5.0×10^{-5}	57	568	10.00	1	0.088	0.157	0.76	0.24	1.80	37	156	512 ³
B4	1.0×10^{-3}	5.0×10^{-5}	27	542	20.00	1	0.084	0.155	0.84	0.16	2.09	23	141	512 ³
C1	2.0×10^{-5}	1.0×10^{-4}	1548	310	0.20	1	0.096	0.155	0.19	0.81	1.30	287	124	512 ³
C2	2.0×10^{-5}	2.0×10^{-4}	1532	153	0.10	1	0.095	0.149	0.14	0.87	1.41	268	76	512 ³
C3	2.0×10^{-5}	4.0×10^{-4}	1516	76	0.05	1	0.094	0.140	0.10	0.90	1.47	248	46	512 ³
X1	5.0×10^{-4}	5.0×10^{-4}	56	56	1.00	0	0.113	0.043	0.46	0.54	0.35	28	29	256 ³
X2	3.5×10^{-5}	3.5×10^{-4}	864	86	0.10	0	0.121	0.039	0.18	0.82	0.26	159	41	256 ³
X3	7.0×10^{-6}	3.5×10^{-4}	4179	84	0.02	0	0.117	0.041	0.08	0.92	0.28	422	42	512 ³
Y1	1.0×10^{-3}	5.0×10^{-5}	55	1093	20.00	0	0.082	0.070	0.44	0.56	2.35	16	164	512 ³
Y2	5.0×10^{-4}	5.0×10^{-5}	121	1213	10.00	0	0.091	0.066	0.40	0.60	1.79	27	168	512 ³
Y3	2.5×10^{-4}	5.0×10^{-5}	245	1227	5.00	0	0.092	0.066	0.38	0.62	1.64	44	167	512 ³
Y4	1.0×10^{-4}	5.0×10^{-5}	647	1293	2.00	0	0.097	0.065	0.33	0.67	1.42	85	171	512 ³
Y5	5.0×10^{-5}	5.0×10^{-5}	1293	1293	1.00	0	0.097	0.062	0.28	0.72	1.32	135	171	512 ³
Y6	2.5×10^{-5}	5.0×10^{-5}	2533	1267	0.50	0	0.095	0.063	0.21	0.79	1.34	210	173	512 ³
Y7	1.0×10^{-5}	5.0×10^{-5}	6400	1280	0.20	0	0.096	0.059	0.12	0.88	1.20	356	174	512 ³

2011b). For $Pr_M \leq 1$, this scaling was also found for small-scale dynamos (Brandenburg 2011a), but now we see that for $Pr_M \geq 1$ the slope is smaller.

Our results for $Pr_M > 1$ are compatible with those of Sahoo et al. (2011), who listed the kinetic and magnetic dissipation scales, $\ell_K = (\nu^3/\epsilon_K)^{1/4}$ and $\ell_M = (\eta^3/\epsilon_M)^{1/4}$, respectively, for their decaying and forced hydromagnetic simulations at different values of Pr_M . Computing the dissipation ratio from their Table 1 as $\epsilon_K/\epsilon_M = Pr_M^3(\ell_K/\ell_M)^{-4}$, we find that their data for non-helical decaying turbulence are well described by the formula $\epsilon_K/\epsilon_M \approx 0.6 Pr_M^{0.55}$. For non-helically forced turbulence with $0.01 \leq Pr_M \leq 10$, their data agree perfectly with our fit $\epsilon_K/\epsilon_M \approx 0.4 Pr_M^{1/3}$ (red filled symbols in Figure 3). In their case, Re_M increases with Pr_M , but its value is generally much larger than our values for $Pr_M < 1$. This suggests that the $1/3$ scaling occurs for large enough magnetic Reynolds numbers and that our steeper fit for $Pr_M \leq 1$ and the mismatch at $Pr_M = 1$ is a consequence of small values of Re_M .

We emphasize that in view of Figure 1, the fraction of energy that is being diverted to magnetic energy through dynamo action depends on the term $-(\mathbf{u} \cdot (\mathbf{J} \times \mathbf{B}))$, and that this must be equal to ϵ_M in the statistically steady state. This fraction is therefore ϵ_M/ϵ_T and we may call it the efficiency of the dynamo. Remarkably, Figure 3 shows that there is a Pr_M dependence of the dynamo efficiency both with and without helicity. The presence of helicity in the forcing function can lead to magnetic field generation at the largest scale of the system. It is therefore also referred to as a large-scale dynamo. Non-helical forcing leads to magnetic fields on scales that are typically somewhat smaller than the energy-carrying scale of the turbulent motions.

One might be worried that these results are artifacts of the Reynolds numbers still being too small and not yet in the asymptotic regime in which a true Pr_M -independence might be expected. However, by comparing the energy spectra in

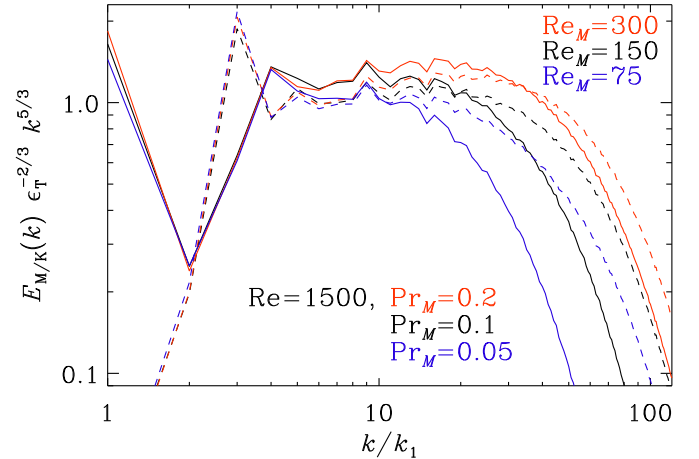


Figure 4. Comparison of compensated kinetic (dashed) and magnetic (solid) energy spectra for $Pr_M = 0.2, 0.1,$ and 0.05 for helically forced turbulence. (A color version of this figure is available in the online journal.)

at least some of the cases indicates that there is indeed a short wavenumber range in which both magnetic and kinetic spectra show an approximate $k^{-5/3}$ scaling with wavenumber k (see Figure 4). On the other hand, however, the presence of a residual slope may also be regarded as evidence that none of the present simulations are yet in the asymptotic regime. Therefore, higher resolution simulations at larger Reynolds numbers remain essential.

The positive slope of the graph of ϵ_K/ϵ_M versus ν/η indicates that a decrease of viscosity ν is not sufficiently compensated by a sharpening of velocity gradients. Likewise, a decrease of η is not fully compensated by a corresponding increase of \mathbf{J}^2 . In other words, as η decreases, and thus $Pr_M (\gg 1)$ is further increased, ϵ_M still decreases and does not remain independent

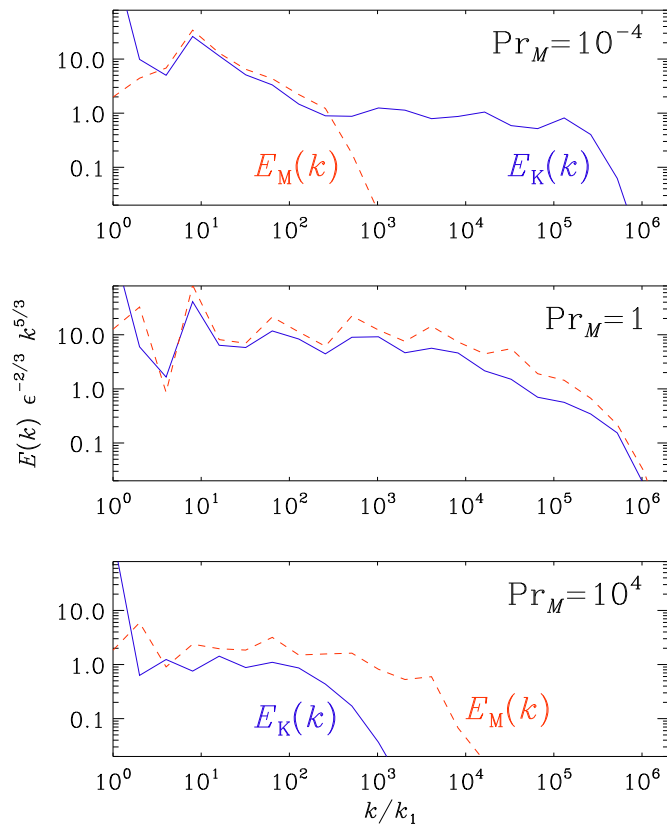


Figure 5. Compensated time-averaged kinetic and magnetic energy spectra for shell models at three values of Pr_M .

(A color version of this figure is available in the online journal.)

of η , as would be the case for $\text{Pr}_M = 1$ (Hendrix et al. 1996). This therefore leads to a residual increase of ϵ_K/ϵ_M . This behavior was partially explained by the findings of Brandenburg (2009, 2011a) that for small values of $\text{Pr}_M = \nu/\eta$, i.e., for $\eta \gg \nu$, most of the spectral energy is dissipated through the magnetic channel, leaving only a reduced amount of kinetic energy to be dissipated, and therefore velocity gradients are not as sharp as in the hydrodynamic case, ϵ_K is reduced, and ϵ_K/ϵ_M decreases with decreasing values of Pr_M .

Before closing the discussion on the Pr_M dependence in three-dimensional MHD turbulence, let us comment on the work term due to fluid expansion. In all of the cases discussed here, $\langle p \nabla \cdot \mathbf{u} \rangle$ turns out to be strongly fluctuating, although its time average is a very small fraction of the total energy (0.02%) for our low Mach number runs (Mach numbers around 0.1). There are indications, however, that $\langle p \nabla \cdot \mathbf{u} \rangle$ is negative for $\text{Pr}_M < 1$ and positive for $\text{Pr}_M > 1$.

Given that there is currently no phenomenological explanation for the scaling of ϵ_K/ϵ_M given by Equation (15), we must consider the possibility that this scaling behavior is not generic and that different scalings can be found in different situations. To shed more light on the possible mechanisms that can explain these scalings, we consider the results of an MHD shell model of turbulence.

3. SHELL MODELS

Shell models represent the dynamics of turbulence using scalar variables for velocity and magnetic field along logarithmically spaced wavenumbers. The governing equations resemble the original ones with diffusion and forcing terms, as well

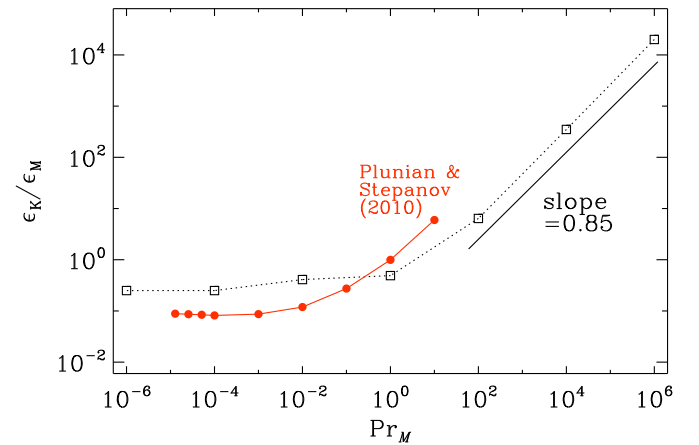


Figure 6. Pr_M dependence of the dissipation ratio for the present shell models (open squares), compared with the shell model results of Plunian & Stepanov (2010), overplotted in red (filled circles).

(A color version of this figure is available in the online journal.)

as quadratic nonlinearities that conserve the same invariants as the original equations: total energy, cross helicity, and a proxy of magnetic helicity. For a recent review of such models, see Plunian et al. (2013). The resulting set of equations can be written as

$$\frac{\partial u_n}{\partial t} = ik_n [N_n(\mathbf{u}, \mathbf{u}) - N_n(\mathbf{b}, \mathbf{b})] - \nu k_n^2 u_n + F_n, \quad (16)$$

$$\frac{\partial b_n}{\partial t} = ik_n [M_n(\mathbf{u}, \mathbf{b}) - M_n(\mathbf{b}, \mathbf{u})] - \eta k_n^2 b_n, \quad (17)$$

where $\mathbf{u} = (u_1, u_2, \dots, u_N)$ and $\mathbf{b} = (b_1, b_2, \dots, b_N)$ are time-dependent complex vectors representing the state of the system at wavenumbers $k_n = 2^n$ with $n = 1, 2, \dots, N$. The nonlinearities are given by (Brandenburg et al. 1996; Frick & Sokoloff 1998)

$$N_n(\mathbf{x}, \mathbf{y}) = x_{n+1}^* y_{n+2}^* - \frac{1}{4} x_{n-1}^* y_{n+1}^* - \frac{1}{8} x_{n-2}^* y_{n-1}^*, \quad (18)$$

$$M_n(\mathbf{x}, \mathbf{y}) = \frac{1}{6} (x_{n+1}^* y_{n+2}^* - x_{n-1}^* y_{n+1}^* - x_{n-2}^* y_{n-1}^*). \quad (19)$$

These equations preserve total energy, cross helicity, and a proxy of magnetic helicity. The only difference between Brandenburg et al. (1996) and Frick & Sokoloff (1998) is a 12/5 scaling factor in front of both nonlinear terms. Models with these coefficients have been used to study the possibility of an inverse cascade in the early universe (Brandenburg et al. 1996, 1997) and the onset properties of small-scale dynamos (Frick & Sokoloff 1998), as well as the possibility of growing dynamo modes from the velocity field of a saturated nonlinear dynamo (Cattaneo & Tobias 2009). Even the Pr_M dependence of the dissipation ratio has already been studied (Plunian & Stepanov 2010; Plunian et al. 2013). Their results show the inverse dissipation ratio in semi-logarithmic form, so the scaling for large Pr_M cannot be accurately assessed, but their results are consistent with a constant dissipation ratio for small Pr_M and show a sub-linear increase at large Pr_M .

To assess the scaling more quantitatively, we now repeat their calculations using an independent method. The time integration is performed using an Adams-Bashforth scheme with

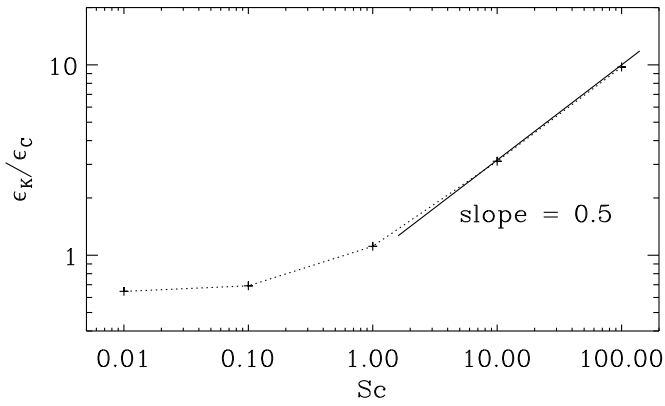


Figure 7. Schmidt number dependence for the passive scalar case.

an integrating factor to treat the diffusion term (Brandenburg et al. 1997). We use $N = 30$ shells for $\text{Re} = u_0/\nu k_0$ of up to 10^9 and Pr_M in the range from 10^{-6} to 10^6 . Forcing is applied by setting F_1 in Equation (16) to a complex random number at each time step, so this forcing is δ -correlated, just like in the DNS. Compensated time-averaged spectra are shown in Figure 5 for three values of Pr_M . For $\text{Pr}_M = 1$, the magnetic and kinetic energy spectra are similar, while for large (small) values of Pr_M , the kinetic (magnetic) energy spectrum is prematurely truncated, as is also the case in the DNS of Brandenburg (2009) for small Pr_M .

As mentioned above, the Pr_M dependence of the dissipation ratio has already been calculated by Plunian & Stepanov (2010), and our present results agree at least qualitatively with theirs. In Figure 6, we show the Pr_M dependence of the dissipation ratio ϵ_K/ϵ_M , where

$$\epsilon_K = 2\nu \sum_{n=1}^N k_n^2 |u_n|^2, \quad \epsilon_M = 2\eta \sum_{n=1}^N k_n^2 |b_n|^2. \quad (20)$$

The present shell models predict the dissipation ratio to be independent of Pr_M for $\text{Pr}_M < 1$, which is in conflict with the DNS of Brandenburg (2009) where this trend was found to continue down to $\text{Pr}_M = 10^{-3}$. On the other hand, the results of Plunian & Stepanov (2010), which are overplotted in Figure 6, suggest a constant dissipation ratio for $\text{Pr}_M \lesssim 0.01$ only, which is already outside the plot range of the present DNS shown in Figure 3, but still in conflict with the DNS of Brandenburg (2009) down to $\text{Pr}_M = 10^{-3}$.

For small values of Pr_M , the present shell models show that the kinetic energy cascade proceeds essentially independently of the magnetic field, just like in ordinary hydrodynamic turbulence. As explained in the Introduction, this is also what one might have naively expected, and it is perhaps even more surprising that this is not borne out by the DNS. On the other hand, for large values of Pr_M , there is actually a fairly strong Pr_M dependence, which is a direct consequence of ϵ_M decreasing for large Re_M rather than a consequence of ϵ_K increasing. Similar results have also been found for a one-dimensional passive scalar model, which will be discussed next and compared with a one-dimensional MHD model, which is an active scalar.

4. DISSIPATION RATIO IN DRIVEN ONE-DIMENSIONAL MODELS

The purpose of this section is to explore the possible behaviors of simple models in which the spatial extent is fully

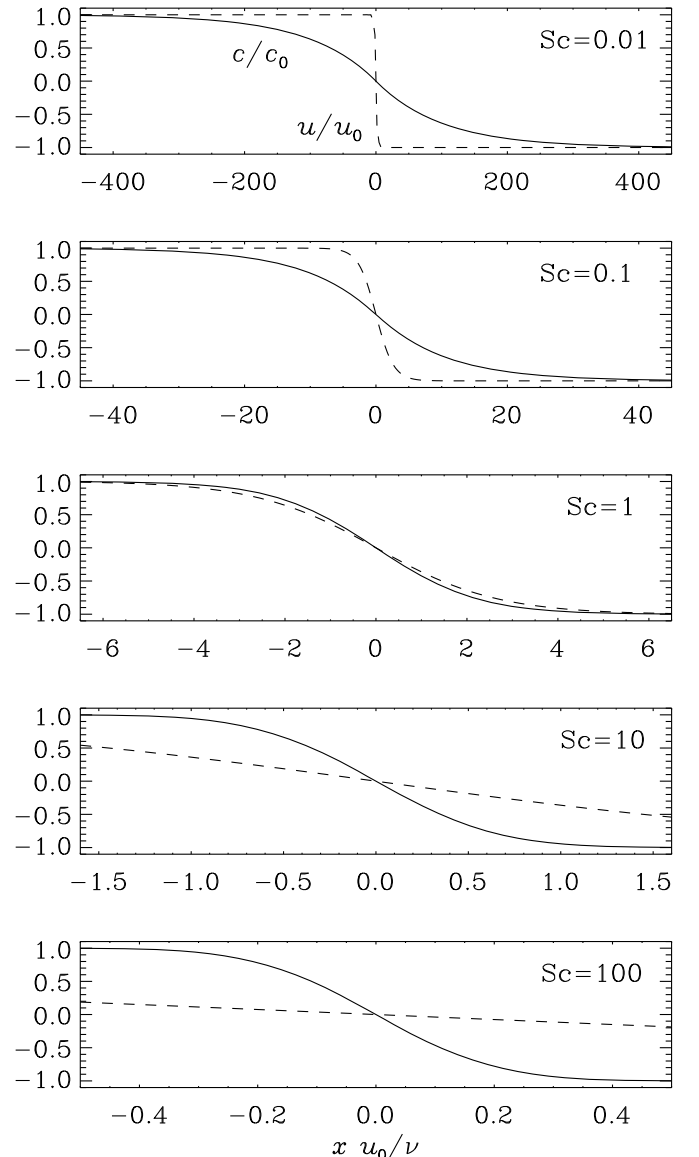


Figure 8. Profiles of $c(x)$ (solid) and $u(x)$ (dashed) for different values of Sc . Note that the x range decreases with increasing values of Sc so as to have a similar coverage of the $c(x)$ profiles in all cases. Note that we have scaled x by u_0/ν , so the hydrodynamic kink always has the same width.

resolved, at least in one dimension. Hydrodynamics in one dimension usually involves shocks, such as the Burgers shock. The pressureless idealization of the hydrodynamic equations is known as the Burgers equation, and solutions can be found in closed form using the Cole-Hopf transformation. Before turning to the magnetic case, we should note that the evolution of a passive scalar field in the presence of a Burgers shock was already considered by Ohkitani & Dowker (2010), who found similar scaling to ours in the limit of a large Schmidt number as $\text{Sc} = \nu/\kappa$, where κ is the passive scalar diffusivity.

4.1. Passive Scalar Model for a Burgers Shock

The passive scalar equation is a simple advection-diffusion equation given by

$$\frac{Dc}{Dt} = \kappa \nabla^2 c, \quad (21)$$

where c is the passive scalar concentration and a relevant passive scalar dissipation is defined as $\epsilon_C = \langle \kappa (\nabla c)^2 \rangle$. For

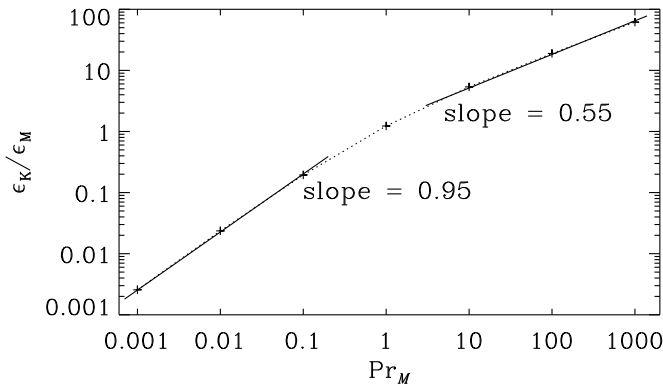


Figure 9. Magnetic Prandtl number dependence in the MHD model.

$Sc \gg 1$, Ohkitani & Dowker (2010) found $\epsilon_K/\epsilon_C \propto Sc^{1/2}$, which is in remarkable agreement with the earlier findings for hydromagnetic turbulence (Brandenburg 2009).

Specifically, the equations considered by Ohkitani & Dowker (2010) are

$$\partial u/\partial t = -uu' + \tilde{\nu}u, \quad (22)$$

$$\partial c/\partial t = -uc' + \kappa c, \quad (23)$$

where primes denotes differentiation with respect to x . The solution to Equation (22) decouples and possesses a shock. In a frame of reference moving with the shock, the solution is stationary and given by

$$u(x) = -u_0 \tanh x/w, \quad (24)$$

where u_0 is the velocity jump and $w_u = 2\tilde{\nu}/u_0$ is the width of the shock with $\tilde{\nu} = 4\nu/3$ as a rescaled viscosity. These equations can be obtained from the hydrodynamic version (i.e., $\mathbf{B} = \mathbf{0}$) of Equation (2) after setting $c_s = 0$, so the density gradient does not enter, and therefore we can ignore Equation (1) and set $\rho = 1$. The $4/3$ factor in the expression for $\tilde{\nu}$ comes from the fact that, owing to compressibility, the viscous acceleration term includes a $(1/3)\nabla\nabla \cdot \mathbf{u}$ term in addition to the usual $\nu\nabla^2\mathbf{u}$ term; see Equation (5) for a corresponding reformulation of the dissipation terms. The viscous dissipation $\epsilon_K = \tilde{\nu} \int (u')^2 dx/L$, using $\partial u/\partial x \propto 1/\cosh^2(x/w)$, is then

$$\epsilon_K = \tilde{\nu} \frac{w}{L} \int \frac{dx/w}{\cosh^4(x/w)} = \frac{4\tilde{\nu}u_0^2}{3wL} = \frac{2u_0^3}{3L}, \quad (25)$$

but here the $4/3$ factor comes from the fact that $\int d\xi/\cosh^4\xi = 4/3$. It is important to note that ϵ_K is constant and independent of ν .

On physical grounds, the passive scalar concentration is positive definite. Mathematically, however, Equation (23) is invariant under the addition of a constant. We can therefore formulate the same boundary conditions for c as for u , i.e., $c = \pm c_0$ and $u = \pm u_0$ for $x \rightarrow \mp\infty$, which is truncated here at finite boundary positions $x = x_{\mp}$ that are chosen to be sufficiently far away from the shock, i.e., $|x_{\pm}| \gg w$.

However, for $Sc \ll 1$, one finds $\epsilon_K/\epsilon_C \approx \text{const}$. The dependence of ϵ_K/ϵ_C as a function of Sc is shown in Figure 7, where we present the results from numerical integration. There are clearly two different scalings for $Sc \ll 1$ and $Sc \gg 1$. The profiles of $c(x)$ are shown in Figure 8 for different values of Sc and are compared with the profile of $u(x)$. Not surprisingly, for small values of Sc , the width of the kink of $c(x)$ becomes wider.

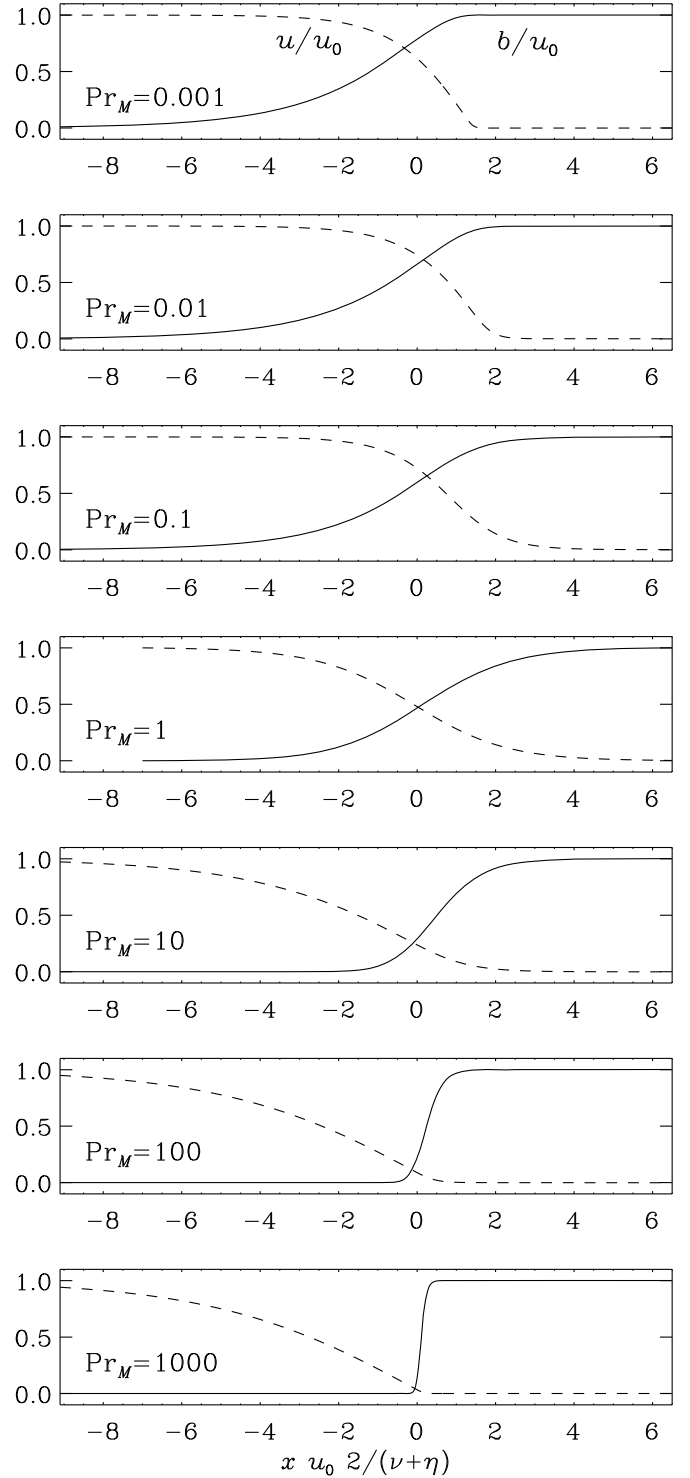


Figure 10. Profiles of $b(x)$ (solid) and $u(x)$ (dashed) for different values of Pr_M . Note that the x range is the same for all panels and that we have normalized x by $2u_0/(\nu + \eta)$.

4.2. MHD Model for Alfvén Kinks

An extension of the Burgers equation to MHD was already studied by Thomas (1968) and Pouquet (1993), but unlike their cases which try to model the effects of three-dimensional dynamos, here we employ just a one-dimensional reduction of the three-dimensional equations to one dimension, which results in equations equivalent to those of Basu et al. (2014).

Table 2
Summary of Runs with $\text{Co} \neq 0$ and $\text{Pr}_M = 0.1$

Run	$\nu k_1/c_s$	$\eta k_1/c_s$	Re	Re_M	Co	u_{rms}/c_s	b_{rms}/c_s	ϵ_K/ϵ_T	ϵ_M/ϵ_T	C_ϵ	k_ν/k_1	k_η/k_1	res.
RA1	1×10^{-3}	1×10^{-2}	30	3	0.1	0.090	0.066	0.30	0.70	1.71	17	4	16^3
RA2	1×10^{-3}	1×10^{-2}	30	3	0.1	0.089	0.064	0.30	0.70	1.68	17	4	16^3
RA3	1×10^{-3}	1×10^{-2}	29	3	0.3	0.088	0.065	0.29	0.71	1.66	17	4	16^3
RA4	1×10^{-3}	1×10^{-2}	29	3	0.6	0.088	0.065	0.29	0.71	1.63	17	4	16^3
RA5	1×10^{-3}	1×10^{-2}	32	3	1.0	0.096	0.063	0.35	0.65	1.31	18	4	16^3
RA6	1×10^{-3}	1×10^{-2}	40	4	2.1	0.121	0.053	0.58	0.42	0.77	21	3	16^3
RB1	5×10^{-4}	5×10^{-3}	56	6	0.1	0.084	0.092	0.16	0.84	2.10	25	7	32^3
RB2	5×10^{-4}	5×10^{-3}	57	6	0.6	0.085	0.094	0.17	0.83	2.03	25	7	32^3
RB3	5×10^{-4}	5×10^{-3}	83	8	2.0	0.124	0.073	0.34	0.67	0.62	30	6	32^3
RC1	2×10^{-4}	2×10^{-3}	150	15	0.6	0.090	0.117	0.13	0.87	1.74	48	14	64^3
RC2	2×10^{-4}	2×10^{-3}	205	21	2.0	0.123	0.100	0.20	0.80	0.66	52	13	64^3
RC3	2×10^{-4}	2×10^{-3}	353	35	4.7	0.212	0.019	0.89	0.11	0.07	65	7	64^3
RD1	1×10^{-4}	1×10^{-3}	310	31	0.5	0.093	0.119	0.13	0.87	1.56	80	23	128^3
RD2	1×10^{-4}	1×10^{-3}	410	41	2.0	0.123	0.127	0.15	0.85	0.69	83	23	128^3
RD3	1×10^{-4}	1×10^{-3}	613	61	5.4	0.184	0.037	0.69	0.31	0.12	105	16	128^3
RE1	5×10^{-5}	5×10^{-4}	647	65	0.5	0.097	0.123	0.14	0.86	1.44	137	39	256^3
RE2	5×10^{-5}	5×10^{-4}	833	83	2.0	0.125	0.134	0.14	0.86	0.69	138	39	256^3
RE3	5×10^{-5}	5×10^{-4}	1160	116	5.8	0.174	0.099	0.39	0.61	0.17	160	32	256^3
RF1	2×10^{-5}	2×10^{-4}	2033	203	2.0	0.122	0.116	0.11	0.89	0.59	243	74	256^3
RF2	2×10^{-5}	2×10^{-4}	2950	295	5.6	0.177	0.106	0.24	0.76	0.14	272	65	256^3
RF3	2×10^{-5}	2×10^{-4}	3917	392	10.6	0.235	0.084	0.42	0.58	0.06	318	62	256^3
RG1	1×10^{-5}	1×10^{-4}	7600	760	10.9	0.228	0.091	0.29	0.71	0.07	501	111	512^3
RG2	1×10^{-5}	1×10^{-4}	6933	693	24.0	0.208	0.089	0.32	0.68	0.09	496	107	512^3

This essentially implies a different sign in front of what corresponds to the stretching term in MHD, i.e., the $\mathbf{B} \cdot \nabla \mathbf{B}$ and $\mathbf{B} \cdot \nabla \mathbf{u}$ non-linearities in the momentum and induction equations, respectively. Unlike the case of a passive scalar, the magnetic field is an active (vector) field which therefore back-reacts on the flow via the Lorentz force, which in this case is just the magnetic pressure. As before, the gas pressure is neglected ($c_s = 0$), so the governing equations therefore reduce to

$$\partial u / \partial t = -uu' - bb' + \tilde{\nu}u'', \quad (26)$$

$$\partial b / \partial t = -ub' - bu' + \eta b''. \quad (27)$$

These equations obey similar conservation equations as the full MHD equation, except that here the energy input comes from non-vanishing inflow at $x \rightarrow -\infty$ and is equal to $u_0^3/3L$. Note, however, that there is no net Poynting flux, because $ub^2 = 0$ on both boundaries.

The magnetic cases are quite different from the passive scalar case in that the magnetic field exerts a magnetic pressure. One can therefore produce a stationary state where the ram pressure of the flow from the left ($x \rightarrow -\infty$) can be balanced by the magnetic pressure of a magnetic kink when $b \rightarrow u_0$ for $x \rightarrow +\infty$ and $b \rightarrow 0$ for $x \rightarrow -\infty$. Indeed, the stationary state must obey the following system of two ordinary differential equations:

$$\partial u / \partial x = (u^2 + b^2 - u_0^2) / 2\tilde{\nu}, \quad (28)$$

$$\partial b / \partial x = ub / \eta. \quad (29)$$

In practice, however, it was more straightforward to obtain solutions using direct time integration in $x_- \leq x \leq x_+$ rather than solving a two-point boundary value problem. The resulting

scaling in Figure 9 confirms Equation (15) with $q \approx 0.55$ for $\text{Pr}_M > 1$ and $q \approx 0.95$ for $\text{Pr}_M < 1$.

Let us now discuss the profiles of $b(x)$ and $u(x)$ in the magnetic case, shown in Figure 10. Here, we find scalings that are broadly similar to those for turbulent large-scale dynamos as well as small-scale dynamos for $\text{Pr}_M < 1$, namely, a slope between 0.6 and 0.7. For $\text{Pr}_M = 1$, the profiles of $b(x)$ and $u(x)$ are similar and resemble the $\tanh x/w$ profile of u in the passive scalar case. However, for both $\text{Pr}_M \ll 1$ and $\gg 1$, the profiles of $b(x)$ and $u(x)$ become asymmetric, which is also the reason why we chose to integrate in a domain where $-x_- > x_+$. For small values of Pr_M , i.e., when $\eta \gg \nu$, the magnetic field begins to ramp up slowly and quite far away from $x = 0$. This leads to a corresponding decline of $u(x)$. On the other hand, for large values of Pr_M , the value of $\nu (\gg \eta)$ is so large that a certain imbalance of $u^2 + b^2 - u_0^2$ in Equation (28) implies only a small slope in $u(x)$, so $|u'|$ must be small.

The crucial point for the magnetic case is that the widths of the magnetic and velocity kinks are never very different from each other. Therefore, as a *zeroth* approximation, we can say that $\langle 2\mathbf{S}^2 \rangle / \langle \mathbf{u}^2 \rangle$ is approximately as large as $\langle \mu_0 \mathbf{J}^2 \rangle / \langle \mathbf{B}^2 \rangle$ or, in our one-dimensional case, $\langle (u')^2 \rangle / \langle u^2 \rangle$ is approximately as large as $\langle (b')^2 \rangle / \langle b^2 \rangle$. Given that in all cases $E_K \approx E_M$, this would imply that $\epsilon_K / \epsilon_M \propto \nu / \eta \equiv \text{Pr}_M$, i.e., we would expect linear scaling with Pr_M . In this case, as we have emphasized before, the usual phenomenology of hydrodynamic turbulence, in which a decrease of ν implies a corresponding increase of dissipation, is not obeyed.

5. EFFECT OF ROTATION

The conversion of kinetic into magnetic energy is of obvious astrophysical significance. In stars with outer convection zones, a certain fraction of the kinetic energy flux is converted into magnetic energy and is observable as X-ray flux (for example,

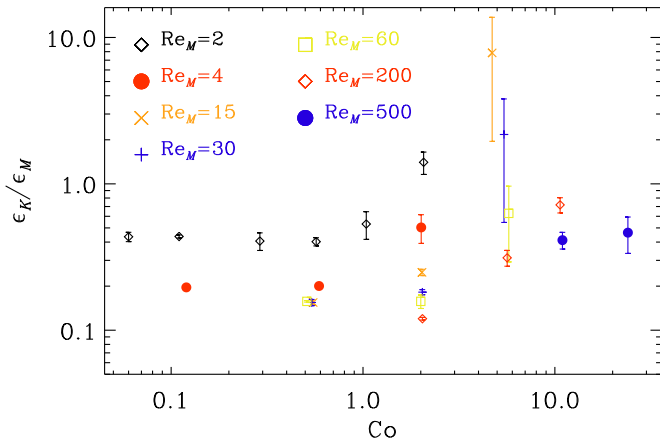


Figure 11. Energy dissipation ratio as a function of the Coriolis number for helically forced turbulence.

(A color version of this figure is available in the online journal.)

(Vilhu 1984)). This leads to a scaling law that has been verified over many orders of magnitude (Christensen et al. 2009). As we have seen, this scaling law must be affected by Pr_M , although the value of Pr_M is approximately the same for all late-type stars, so this cannot easily be observationally checked. However, what has not been checked is whether the conversion also depends on the rotation rate.

In the work discussed in Section 2, there was no explicit rotation. Note, however, that Plunian & Stepanov (2010) did already study the effect of rotation in their shell model calculations. To check whether rotation influences our results, we have performed a series of simulations with $\text{Co} \neq 0$ using $\text{Pr}_M = 1$, and have varied $\text{Re}_M (= \text{Re})$ between 4 and 400, and Co between 0.2 and 20. The parameters of our runs are listed in Table 2 and the result is shown in Figure 11, where we plot ϵ_K/ϵ_M as a function of Co . The values of Re_M are indicated by different symbols.

We see that for a given value of Re_M , there is a certain value of $\text{Co} = \text{Co}^*$ below which ϵ_K/ϵ_M is roughly unaffected by rotation. As the value of Re_M is increased, Co^* also increases, thereby extending the range over which ϵ_K/ϵ_M remains roughly independent of Co . In astrophysical applications, Re is usually large enough so that we should not expect to see any rotational dependence of ϵ_K/ϵ_M . This explains why the scaling result of Christensen et al. (2009) follows the expected scaling of $\epsilon_K + \epsilon_M \approx u_{\text{rms}}^3/L$ with some length scale L over a huge range.

6. CONCLUSIONS

In the present work, we have extended earlier findings of a Pr_M dependence of the kinetic-to-magnetic energy dissipation ratio, ϵ_K/ϵ_M , to the regime of small-scale and large-scale dynamos for $\text{Pr}_M > 1$ and at higher resolution than what was previously possible (Brandenburg 2011b). In most cases, our results confirm earlier results that for large-scale dynamos, the ratio ϵ_K/ϵ_M is proportionate to $\text{Pr}_M^{0.6}$. Furthermore, we have shown that a similar scaling with Pr_M can be obtained for a simple one-dimensional Alfvén kink, where ram pressure locally balances magnetic pressure. Interestingly, in these cases, kinetic energy dissipation is accomplished mainly by the irrotational part of the flow rather than the solenoidal part, as in the turbulence simulations presented here. We note in this connection that the kinetic energy dissipation, which is proportional to

$\langle 2\mathbf{S}^2 \rangle = \langle (\nabla \times \mathbf{u})^2 \rangle + \langle (4/3)(\nabla \cdot \mathbf{u})^2 \rangle$, has similar contributions from vortical and irrotational parts.

We have also shown that for fixed values of Pr_M , the ratio ϵ_K/ϵ_M is not strongly dependent on the presence of rotation, provided the magnetic Reynolds number is not too close to the marginal value for the onset of dynamo action. In the simulations with $\text{Co} \neq 0$ presented here, the runs were often not very long and therefore the error bars large, but the number of similar results support our conclusions that ϵ_K/ϵ_M is roughly independent of Co .

For many astrophysical systems, the microscopic energy dissipation mechanism is not of Spitzer type, as assumed here. It is not obvious how this would affect our results. Nevertheless, it is clear that conclusions based on the kinetic-to-magnetic energy ratio itself do not have much bearing on the energy dissipation ratio. This became clear some time ago in connection with local accretion disk simulations driven by the magneto-rotational instability, where magnetic energy strongly dominates over kinetic. However, as it turned out, most energy is dissipated viscously rather than resistively (Brandenburg et al. 1995).

Unfortunately, the question of energy dissipation is not routinely examined in astrophysical fluid dynamics, nor is it always easy to determine energy dissipation rates, because many astrophysical fluid codes ignore explicit dissipation and rely entirely on numerical prescriptions needed to dissipate energy when and where needed. Our present work highlights once again that this can be a questionable procedure, because it means that even non-dissipative aspects, such as the strength of the dynamo which is characterized by $\langle \mathbf{u} \cdot (\mathbf{J} \times \mathbf{B}) \rangle$, are then ill-determined. The reason why this has not been noted earlier is that most previous work assumed Pr_M to be of the order of unity. An exception is the work of Brandenburg (2009), where dynamo simulations for values of Pr_M as small as 10^{-3} were considered. One reason why such extreme values of Pr_M have been possible is the fact that at very small values of Pr_M , most of the energy is dissipated resistively and there is not much kinetic energy left at the end of the turbulent kinetic energy cascade. As a consequence, it is then possible to decrease the value of ν further and still dissipate the remaining kinetic energy, which implies that the nominal value of the fluid Reynolds number can become much larger than what is usually possible when there is no additional resistive dissipation. However, one may wonder how a large-scale dynamo can depend on Pr_M . We expect that this is only possible if most of the energy transfer comes ultimately from small scales.

It is also noteworthy that there is now some evidence for the non-universal behavior of the scaling of the kinetic-to-magnetic energy dissipation ratio with Pr_M . Although some of the earlier results with slightly different exponents could be explained by inaccuracies and other physical effects, there are now examples such as one-dimensional simulations and the passive scalar analogy that display different exponents which cannot easily be explained through artifacts. Also, the result that for large enough magnetic Reynolds numbers the dissipation ratio scales differently in the presence of helicity ($q \approx 0.7$) than without ($q \approx 1/3$) is surprising. It would therefore be interesting to revisit the viscous-to-magnetic dissipation ratios over a broader range of circumstances.

I thank Koji Ohkitani for useful discussions and Rodion Stepanov for comments on the paper and for providing the dissipation rates found in his paper with Franck Plunian, which are now overplotted in Figure 6 of the present paper. I also

thank Prasad Perlekar for referring me to the data of their paper of 2011, which are now overplotted in Figure 3 of the present paper. This work was supported in part by the European Research Council under the AstroDyn Research Project No. 227952, and the Swedish Research Council grants No. 621-2011-5076 and 2012-5797, as well as the Research Council of Norway under the FRINATEK grant 231444. We acknowledge the allocation of computing resources provided by the Swedish National Allocations Committee at the Center for Parallel Computers at the Royal Institute of Technology in Stockholm and the National Supercomputer Centers in Linköping, the High Performance Computing Center North in Umeå, and the Nordic High Performance Computing Center in Reykjavik.

REFERENCES

- Balbus, S. A., & Hawley, J. F. 1998, *RvMP*, **70**, 1
 Basu, A., Naji, A., & Pandit, R. 2014, *PhRvE*, **89**, 012117
 Bisnovatyi-Kogan, G. S., & Lovelace, R. V. E. 1997, *ApJL*, **486**, L43
 Boldyrev, S., & Cattaneo, F. 2004, *PhRvL*, **92**, 144501
 Brandenburg, A. 2001, *ApJ*, **550**, 824
 Brandenburg, A. 2009, *ApJ*, **697**, 1206
 Brandenburg, A. 2011a, *ApJ*, **741**, 92
 Brandenburg, A. 2011b, *AN*, **332**, 51
 Brandenburg, A., Enqvist, K., & Olesen, P. 1996, *PhRvD*, **54**, 1291
 Brandenburg, A., Enqvist, K., & Olesen, P. 1997, *PhLB*, **392**, 395
 Brandenburg, A., Nordlund, Å., Stein, R. F., & Torkelsson, U. 1995, *ApJ*, **446**, 741
 Brandenburg, A., & Subramanian, K. 2005, *A&A*, **439**, 835
 Candelaresi, S., & Brandenburg, A. 2013, *PhRvE*, **87**, 043104
 Candelaresi, S., Hubbard, A., Brandenburg, A., & Mitra, D. 2011, *PhPI*, **18**, 012903
 Cattaneo, F., & Tobias, S. M. 2009, *JFM*, **621**, 205
 Cho, J., & Vishniac, E. T. 2000, *ApJ*, **538**, 217
 Christensen, U. R., Holzwarth, V., & Reiners, A. 2009, *Natur*, **457**, 167
 Frick, P., & Sokoloff, D. 1998, *PhRvE*, **57**, 4155
 Fromang, S., & Papaloizou, J. 2007, *A&A*, **476**, 1113
 Fromang, S., Papaloizou, J., Lesur, G., & Heinemann, T. 2007, *A&A*, **476**, 1123
 Galsgaard, K., & Nordlund, Å. 1996, *JGR*, **101**, 13445
 Haugen, N. E. L., Brandenburg, A., & Dobler, W. 2003, *ApJL*, **597**, L141
 Haugen, N. E. L., Brandenburg, A., & Dobler, W. 2004, *PhRvE*, **70**, 016308
 Hawley, J. F., Gammie, C. F., & Balbus, S. A. 1996, *ApJ*, **464**, 690
 Hendrix, D. L., van Hoven, G., Mikic, Z., & Schnack, D. D. 1996, *ApJ*, **470**, 1192
 Isakov, A. B., Schekochihin, A. A., Cowley, S. C., McWilliams, J. C., & Proctor, M. R. E. 2007, *PhRvL*, **98**, 208501
 Käpylä, P. J., & Korpi, M. J. 2011, *MNRAS*, **413**, 901
 Kazantsev, A. P. 1968, *JETP*, **26**, 1031
 Mininni, P. D. 2007, *PhRvE*, **76**, 026316
 Ohkitani, K., & Dowker, M. 2010, *JMPH*, **51**, 033101
 Plunian, F., & Stepanov, R. 2010, *PhRvE*, **82**, 046311
 Plunian, F., Stepanov, R., & Frick, P. 2013, *PhR*, **523**, 1
 Pouquet, A. 1993, in *Astrophysical Fluid Dynamics*, ed. J.-P. Zahn & J. Zinn-Justin (Amsterdam: North-Holland), 139
 Rogachevskii, I., & Kleeorin, N. 1997, *PhRvE*, **56**, 417
 Sahoo, G., Perlekar, P., & Pandit, R. 2011, *NJPh*, **13**, 013036 (SPP11)
 Schekochihin, A. A., Cowley, S. C., Taylor, S. F., Maron, J. L., & McWilliams, J. C. 2004, *ApJ*, **612**, 276
 Schekochihin, A. A., Haugen, N. E. L., Brandenburg, A., et al. 2005, *ApJL*, **625**, L115
 Schekochihin, A. A., Isakov, A. B., Cowley, S. C., et al. 2007, *NJPh*, **9**, 300
 Schekochihin, A. A., Maron, J. L., Cowley, S. C., & McWilliams, J. C. 2002, *ApJ*, **576**, 806
 Shakura, N. I., & Sunyaev, R. A. 1973, *A&A*, **24**, 337
 Stone, J. M., Hawley, J. F., Gammie, C. F., & Balbus, S. A. 1996, *ApJ*, **463**, 656
 Thomas, J. H. 1968, *PhFl*, **11**, 1245
 Tran, C. V., Yu, X., & Blackburn, L. A. K. 2013, *JFM*, **725**, 195
 Vilhu, O. 1984, *A&A*, **133**, 117